HHS Public Access

Author manuscript

Anticancer Res. Author manuscript; available in PMC 2015 June 03.

Published in final edited form as:

Anticancer Res. 2010 November ; 30(11): 4415–4422.

Real-time Imaging of Tumor Progression in a Fluorescent Orthotopic Mouse Model of Thyroid Cancer

HOP S. TRAN CAO[1], **SHARMEELA KAUSHAL**[2], **CYNTHIA S. SNYDER**[2], **WEG M. ONGKEKO**[1], **ROBERT M. HOFFMAN**[1,2,3], and **MICHAEL BOUVET**[1,2]

[1]Department of Surgery, University of California San Diego, San Diego, CA, U.S.A

[2]Moores Cancer Center, University of California San Diego, San Diego, CA, U.S.A

[3]AntiCancer Inc., San Diego, CA, U.S.A

Abstract

There is a need for a clinically relevant mouse model of thyroid cancer that enables real-time, non-invasive monitoring of tumor growth, progression, and drug response over time. Human thyroid cancer cell lines NPA (papillary) and KAK-1 (anaplastic) were stably transfected to express either red or green fluorescent protein. Cancer cells were injected into the thyroid glands of 8-week-old athymic mice. The animals were imaged with whole-body fluorescence imaging weekly and sacrificed when premorbid. At necropsy, the primary tumor was resected en bloc with the respiratory system for processing and analysis. Histology was performed on fixed tissue specimens for review of morphologic findings. Both anaplastic and papillary thyroid cancer cell lines led to robust development of orthotopic fluorescent tumors in nude mice. Injection of 5×10^5 cancer cells was sufficient for tumor development. Tumors were visualized for both cell lines via non-invasive imaging as early as 3 weeks post-implantation and were monitored over time. Time to premorbid condition varied between mice and was associated with a primary tumor growth pattern (early local compression of the esophagus vs. late metastatic disease) rather than tumor size. At necropsy, tumor fluorescence demonstrated metastases in the lungs, lymph nodes and vessels that were not visible under white light. Thus an orthotopic mouse model of thyroid cancer has been developed that replicates the major clinical features of thyroid cancer and enables real-time, non-invasive monitoring of tumor progression. This model should permit preclinical evaluation of novel thyroid cancer therapeutics.

Keywords

Fluorescent proteins; nude mice model; metastasis; NPA; KAK-1; GFP; thyroid cancer

Thyroid cancer is diagnosed in approximately 40,000 Americans and causes over 1,600 deaths annually (1). The most common type is papillary thyroid carcinoma (PTC), comprising nearly 70% of all thyroid cancer cases. PTC has a favorable prognosis, especially when detected early, when five-and ten-year survival rates exceed 90% (2).

Correspondence to: Michael Bouvet, MD, Moores UCSD Cancer Center, 3855 Health Sciences Drive #0987, La Jolla, CA 92093-0987, U.S.A. Tel: +1 8588226191, Fax: +1 8588226192, mbouvet@ucsd.edu.

However, in its advanced stages, survival rates are reduced nearly by half. In contrast, anaplastic thyroid cancer (ATC) remains one of the most lethal types of cancer, with most patients surviving only 6 months from the time of diagnosis (3). Its aggressive nature, frequent late presentation, and tendency to metastasize early account for this virulent profile, and currently no effective treatment exists.

In recent years, common genetic alterations found in PTC have been identified that modulate RET and BRAF kinases (4, 5). This latter mutation is also involved in ATC (6), reflecting its development from well-differentiated thyroid cancer through anaplastic transformation (7). As efforts to develop targeted therapies against these kinases are pursued, it is important that appropriate animal models be available to evaluate them *in vivo*. It is generally recognized that orthotopic animal models of human cancer are the optimal tool for preclinical evaluation of novel therapeutics, since they best recapitulate the disease process in humans (8, 9). In the case of thyroid cancer, such a model was first reported in 2005 by Kim *et al.*, who developed an orthotopic model of human ATC in athymic nude mice (10).

The current authors have pioneered the use of fluorescent proteins for *in vivo* imaging and have applied this technology to orthotopic animal models of human cancer, enabling real-time, non-invasive imaging of tumor growth, progression, and metastasis (11–13). Tumors labeled with green fluorescent protein (GFP) or red fluorescent protein (RFP) can be followed over time in a live animal by non-invasive imaging, negating the need to sacrifice or operate on the animal to assess tumor behavior. In addition, assessment of metastatic disease is more accurate with the use of fluorescent proteins, as small metastatic deposits or those embedded in normal tissue of similar color and composition can be detected by their fluorescence. This can be especially helpful in the case of metastasis to the lungs, a common site of distal spread in thyroid cancer.

In the present study, a fluorescent orthotopic mouse model of two types of human thyroid cancer, PTC and ATC, was developed. This model allows monitoring of thyroid tumors over time and improved diagnostic evaluation of metastatic burden at the time of necropsy. This model will serve as a useful tool in the evaluation of novel therapeutics in the treatment of thyroid cancer.

Materials and Methods

Cell culture

The human cell lines NPA (papillary thyroid cancer) and KAK-1 (anaplastic thyroid cancer) were maintained in Dulbecco's modified Eagle's medium (DMEM) (Gibco-BRL, Grand Island, NY, USA) supplemented with 10% fetal bovine serum (Hyclone, Logan, UT, USA), penicillin/streptomycin (Gibco-BRL), sodium pyruvate (Gibco-BRL), sodium bicarbonate (Cellgro, Manassas, VA, USA), L-glutamine (Gibco-BRL), and MEM non-essential amino acids (Gibco-BRL). All cells were incubated at 37°C with 5% CO_2.

Production of stable red and green fluorescent cell lines (NPA-RFP and KAK-1-RFP; KAK-1-GFP)

Highly fluorescent, RFP- or GFP-expressing thyroid cancer cell lines were generated as previously described (12). Briefly, the pDSRed-2 vector (Clontech Laboratories, Inc., Palo Alto, CA, USA) was used to engineer clones of NPA and KAK-1 cells that stably express RFP, while the stable GFP-expressing KAK-1 cell line was generated with the use of the pLEIN-GFP vector (Clontech Laboratories, Inc.) (11, 14).

Animal care

Twelve female athymic *nu/nu* nude mice were maintained in a barrier facility on high efficiency particulate air (HEPA)-filtered racks. The animals were fed with autoclaved laboratory rodent diet (Teckland LM-485; Western Research Products, Orange, CA, USA). All surgical procedures were performed under anesthesia with an intramuscular injection of 100 μl of a mixture of 100 mg/kg ketamine and 10 mg/kg xylazine. For each procedure, 20 μl of 1 mg/kg buprenorphine was administered for pain control. Euthanasia was achieved by 100% carbon dioxide inhalation, followed by cervical dislocation. All animal studies were approved by the UCSD Institutional Animal Care and Use Committee and conducted in accordance with principles and procedures outlined in the NIH Guide for the Care and Use of Animals.

Orthotopic thyroid cancer model

NPA-RFP, KAK-1-RFP, and KAK-1-GFP cells were harvested by trypsinization and washed three times with serum-free medium. Viability was verified to be greater than 95% for each cell line using the Vi-Cell XR automated cell viability analyzer (Beckman Coulter, Brea, CA, USA). To determine necessary cell numbers for tumor growth, cells were resuspended at either 5×10^5 or 5×10^6 per 5 μl of serum-free medium and placed on ice prior to implantation. Orthotopic models were established in four groups of three 8-week old female mice with the aid of surgical loupes of magnification 2.5×. The four groups included: (i) KAK-1-RFP: 5×10^6 cells; (ii) KAK-1-RFP: 5×10^5 cells; (iii) NPA-RFP: 5×10^5 cells; and (iv) KAK-1-GFP: 5×10^5 cells. After anesthesia was administered as described above, a 1.0- to 1.5-cm longitudinal midline cervical incision was made in the anterior neck of the mouse. The salivary glands were retracted laterally, and the underlying superficial strap muscles gently teased off the midline, revealing the trachea and the two flanking thyroid glands. The deeper strap muscles were left intact on the trachea to assist in exposing the glands for tumor cell injection by tracheal rotation. A 25-μl Hamilton syringe (Hamilton Company, Reno, NV, USA) fitted with a 26-gauge needle was used to inject the cells directly into one or both of the thyroid glands. The total volume injected in each gland was 5 μl, containing 5×10^6 or 5×10^5 cells. The submandibular glands were then returned to the midline position, and the skin was closed in a single layer in a running fashion using a 6.0 Ethibond non-absorbable suture (Ethicon Inc., Somerville, NJ, USA).

Animal imaging and necropsy

After orthotopic implantation, mice were imaged weekly with the Olympus OV100 Small Animal Imaging System (Olympus Corp., Tokyo, Japan) equipped with an MT-20 light

source (Olympus Biosystems, Planegg, Germany) and a DP71 CCD color camera (Olympus Corp.) that is interchangeable with an ImagEM-CCD monochrome digital camera (Hamamatsu Photonics K.K., Hamamatsu City, Japan). The imaging chamber was mounted with a gas nose cone that delivers a steady flow of a mixture of isofluorane gas and 100% oxygen directly to the mouse to keep it anesthetized. Both bright light and fluorescent images were obtained.

The animals were sacrificed when they either reached premorbid conditions, as defined by a combination of cachexia and diminished activity level, or at certain preset time points, whichever came first. The five, ten and fifteen weeks post-implantation marks were chosen as time points at which one mouse of each group would be sacrificed.

At the time of euthanasia, a midline sternotomy extending from the xiphoid process up to the base of the mandible was performed, so as to expose the thyroid glands and tumors in continuity with the airways and the lungs within the chest cavity. The tumor was resected *en bloc* with the respiratory system, starting most rostrally at the level of the thyroid cartilage and including the lungs caudally. The specimen was imaged under both bright light and fluorescent light modes with the OV100.

Histology

The thyroid/tumor and respiratory system organ block was either fixed in Bouin's solution and embedded in paraffin prior to sectioning and staining with H&E for standard light microscopy or frozen in OCT for examination under fluorescence microscopy. H&E-stained permanent sections were examined using an Olympus BX41 microscope equipped with a Micropublisher 3.3 RTV camera (QImaging, Surrey, BC, Canada). All images were acquired using QCapture software (QImaging) without post-acquisition processing. Fluorescence microscopy was performed using an inverted Nikon DE-300 microscope and Spot camera RD (Tokyo, Japan).

Data processing

All whole-body and macroscopic images were analyzed using Image-J (National Institute of Health Bethesda, MD, USA) and were processed for contrast and brightness with the use of Photoshop Element-4 (Adobe Systems Inc. San Jose, CA, USA).

Results

All animals tolerated the surgical implantation well, without any surgery- or anesthesia-related complications. After injection of the fluorescent tumor cells into the thyroid glands, fluorescence imaging was used to confirm accumulation of the cells in the correct location. Both NPA and KAK-1 cell lines exhibited 100% tumorigenicity after intra-thyroid cell injection. Injection of 5×10^5 KAK-1-RFP cells and 5×10^6 KAK-1-RFP cells both achieved 100% tumor growth, with no significant difference in growth pattern and nearly identical growth timelines observed. The earliest time to detection of tumor growth based on non-invasive fluorescence imaging was 21 days post-implantation in a mouse bearing a KAK-1-RFP tumor (5×10^6 cells), while the latest time to imageable tumor growth was 11 weeks post-implantation in a mouse with a NPA-RFP tumor. The median time to imageable tumor

detection for RFP-expressing KAK-1 cells was five weeks post-implantation, and nine weeks post-implantation for the NPA cell line.

RFP conferred a definitive advantage over GFP for transcutaneous tumor detection in the cervical area. Unlike GFP-expressing tumors, it was possible to detect RFP-expressing tumors by imaging well before they became palpable and it was possible to monitor their progression over weeks, providing a timeline of tumor growth in the live animals (Figure 1).

While tumors grew in all mice, it was the tumors' growth patterns and not their sizes that appeared to determine survival. For both NPA and KAK-1, some tumors grew primarily in an exophytic fashion and were associated with longer survival, while other tumors caused esophageal compression early in the disease course, leading to rapid deterioration and resulting in early cachexia and mortality in these animals. The pattern of tumor growth appeared to be stochastic and was not associated with the tumor type (NPA *vs*. KAK-1) or number of cells injected (5×10^5 *vs*. 5×10^6 cells).

Upon necropsy, fluorescence imaging of the exposed thyroid gland and respiratory tract allowed rapid identification of a bright primary tumor in each thyroid gland (Figure 2). Mice that became premorbid early due to esophageal compression failed to develop metastases. In contrast, mice in which tumors grew in an exophytic fashion were sacrificed at later dates, at which point they tended to have larger primary tumors and multiple associated metastases. Most common sites of metastasis included the paratracheal lymph nodes and the lungs (Figure 3A). These RFP-expressing metastatic lesions were easily detectable with fluorescence imaging but essentially undetectable under white light microscopy (Figure 3B). Furthermore, fluorescence imaging at higher magnifications permitted visualization of single cancer cells within small, superficial vascular structures traversing the pleural surface of the lung parenchyma (Figure 4). Primary and metastatic KAK-1-GFP lesions were also visualized with fluorescence imaging at necropsy (Figure 5).

After completion of intravital imaging, tumors were removed *en bloc* with the respiratory track and processed for histology. The cartilaginous tracheal rings were readily identified in H&E-stained transverse sections of the thyroid tumors (Figures 6A, C). A thin rim of normal thyroid tissue, distinguished by its characteristic colloid-filled follicles, was found partially encircling the anterior aspect of the trachea. Orthotopically implanted, fluorescent protein-expressing tumor cells formed discreet tumor masses of various sizes which distorted adjacent normal tissues and sometimes caused compression of the esophagus (Figure 6A, arrow). The histologic features of the tumors varied, with KAK-1 tumors demonstrating extensive central necrosis and less evidence of differentiation (Figures 6A, B). Tumors developing from NPA cells were better differentiated but less well-demarcated, with focally infiltrative tumor margins and a tendency to involve small vessels near the tumor (Figures 6C, D).

Discussion

As new potential therapeutic targets for thyroid cancer are identified, novel drugs and treatment strategies will be developed that require an appropriate animal model for their

evaluation. Ideally, such a model would resemble the disease process in humans both clinically and pathologically, allow for the tumor response to therapy to be monitored over time in a live animal, and afford easy and accurate detection of disease progression at the time of necropsy. It is now clear that orthotopic mouse models of human cancer are vastly superior to their subcutaneous xenograft counterparts, because the former provide the best representation of the disease process in patients (8, 9). Kim *et al.* (10) demonstrated in their orthotopic model of ATC that the clinical features of the disease and the metastatic pattern obtained in mice recapitulated those found in human ATC. Furthermore, they showed that the orthotopic model resulted in significantly greater tumorigenicity and promoted greater angiogenesis than the subcutaneous model. The clinical applicability of this model allowed them to subsequently investigate a number of therapeutics against ATC (15–20). Likewise, an orthotopic model of PTC described by Ahn *et al.* led to the development of metastases to the cervical lymph nodes and lungs, as occurs clinically but not in subcutaneous PTC models (21). In the current study, orthotopic implantation of both NPA and KAK-1 cells into the mouse thyroid glands resulted in a model which accurately recapitulates the clinically relevant features of human PTC and ATC, namely local tissue invasion, compression of adjacent organs, development of cachexia, and metastastic disease to paratracheal lymph nodes and the lungs.

Non-fluorescent orthotopic models of thyroid cancer, however, are limited with regard to continuous monitoring of tumor progression and response to therapy. Ahn *et al.* (21) reported that orthotopically-growing tumors are located deep in the neck and are difficult to detect. Moreover, transcutaneous measurement of the deeply-growing thyroid tumors is challenging and inaccurate. Tumors labeled with fluorescent proteins, on the other hand, can be imaged accurately over time in orthotopic models. Our laboratory previously demonstrated that imaging with fluorescent protein correlates well with both ultrasound and magnetic resonance imaging evaluation of primary tumors in orthotopic mouse models of pancreatic cancer (22, 23). In the current study, RFP-expressing NPA and KAK-1 tumors were detectable in the neck transcutaneously *via* whole-body imaging long before they became palpable. Monitoring of tumor progression was achievable from the onset of tumor detection until the animals were sacrificed.

Finally, detection of small metastatic lesions can be challenging, especially if they are present within the lung parenchyma and not on the lung surface. The same problem is encountered when tumor deposits are surrounded by or located within tissues of the same color and composition. These problems are mostly circumvented when tumors are fluorescently labeled, when even single-cell level metastases can be detected (24). Nucera *et al.* recently described a GFP-expressing orthotopic mouse model of ATC in which GFP expression facilitated detection of multifocal pulmonary micrometastases (25). However, in their study, no non-invasive real-time imaging was performed. In the present study, RFP enabled non-invasive imaging of the tumor, conferring the major advantage of real-time monitoring of tumor growth and progression. Furthermore, metastases to the paratracheal lymph nodes and to the lungs that were undetectable under bright light were brightly fluorescent in the current model. Thus, some animals that would have been considered to have local disease only without the use of fluorescent proteins had metastatic lesions that

were identified *via* fluorescence imaging. Not visualizing existing metastases would obviously have a significant impact on the evaluation of novel therapeutics by understaging the disease, or conversely, overestimating the efficacy of the therapy being tested. The application of fluorescence imaging would therefore greatly diminish the potential for such errors to occur.

Schweppe *et al.* (26) used short tandem repeat profiling and single nucleotide polymorphism array analysis on a series of thyroid cancer cell lines. These authors claim that KAK-1 is a derivative of the HT-29 colon cancer cell line and the NPA is a derivative of the MDA-MB-435 cell line which they term melanoma but is in reality a breast cancer cell line (27, 28).

However, this characterization by Schweppe *et al.* seems unlikely. First of all, NPA is a human PTC developed by Juillard at UCLA (29) and KAK-1 is a human ATC developed by Fusco (30, 31). Secondly, both the HT-29 (32) and MDA-MB-435 (33, 34) cell lines are relatively indolent, in sharp contrast to the highly aggressive and metastatic behavior observed for NPA and KAK-1 in the current study. The pattern of orthotopic primary tumor growth and metastasis of NPA and KAK-1 reflect the clinical pattern of thyroid carcinoma.

In addition, if these cell lines were indeed not of thyroid origin, their ectopic implantation on the thyroid should make them even more indolent (35), in sharp contrast to the highly aggressive behavior observed for NPA and KAK-1, in the current study, indicating NPA and KAK-1 are cancer cell lines of thyroid origin and the thyroid is the orthotopic organ. Moreover, the KAK-1 tumors demonstrated extensive central necrosis and less evidence of differentiation and tumors developing from NPA cells were better differentiated in the current study. This is consistent with the anaplastic character of KAK-1 and the papillary character of NPA, respectively, again indicating that NPA and KAK-1 are thyroid carcinoma cell lines.

In conclusion, in this study a novel, imageable, fluorescent orthotopic mouse model of human papillary and anaplastic thyroid cancers was developed. By combining RFP fluorescence imaging and orthotopic implantation, this model gains three major strengths, making it uniquely useful in the evaluation of thyroid cancer. First, it recapitulates the disease process in humans both clinically and pathologically. Second, it allows for tumor progression and response to investigational therapies to be non-invasively monitored and followed over time in a live animal. And third, it permits facile and reliable detection of metastatic disease, even at the single-cell level, that can otherwise be missed with bright lighting, thereby resulting in more accurate disease staging. The current model should serve as an ideal preclinical system in which to evaluate novel therapeutics for thyroid cancer and help provide a powerful insight into the tumor biology of this disease.

Acknowledgments

This study was supported in part by grants from the National Cancer Institute CA109949 (to M.B.) and CA132971 (to M.B. and Anticancer Inc.) and American Cancer Society RSG-05-037-01-CCE, T32 training grant CA121938 (to H.S. T.C.).

References

1. Jemal A, Siegel R, Ward E, Hao Y, Xu J, Thun MJ. Cancer statistics, 2009. CA Cancer J Clin. 2009; 59:225–249. [PubMed: 19474385]
2. Eichhorn W, Tabler H, Lippold R, Lochmann M, Schreckenberger M, Bartenstein P. Prognostic factors determining long-term survival in well-differentiated thyroid cancer: an analysis of four hundred eighty-four patients undergoing therapy and aftercare at the same institution. Thyroid. 2003; 13:949–958. [PubMed: 14611704]
3. Chiacchio S, Lorenzoni A, Boni G, Rubello D, Elisei R, Mariani G. Anaplastic thyroid cancer: prevalence, diagnosis and treatment. Minerva Endocrinol. 2008; 33:341–357. [PubMed: 18923370]
4. Nikiforov YE. RET/PTC rearrangement in thyroid tumors. Endocr Pathol. 2002; 13:3–16. [PubMed: 12114746]
5. Xing M. *BRAF* mutation in papillary thyroid cancer: pathogenic role, molecular bases, and clinical implications. Endocr Rev. 2007; 28:742–762. [PubMed: 17940185]
6. Begum S, Rosenbaum E, Henrique R, Cohen Y, Sidransky D, Westra WH. *BRAF* mutations in anaplastic thyroid carcinoma: implications for tumor origin, diagnosis and treatment. Mod Pathol. 2004; 17:1359–1363. [PubMed: 15195111]
7. Wiseman SM, Loree TR, Hicks WL Jr, Rigual NR, Winston JS, Tan D, Anderson GR, Stoler DL. Anaplastic thyroid cancer evolved from papillary carcinoma: demonstration of anaplastic transformation by means of the inter-simple sequence repeat polymerase chain reaction. Arch Otolaryngol Head Neck Surg. 2003; 129:96–100. [PubMed: 12525202]
8. Bibby MC. Orthotopic models of cancer for preclinical drug evaluation: advantages and disadvantages. Eur J Cancer. 2004; 40:852–857. [PubMed: 15120041]
9. Hoffman RM. Orthotopic metastatic mouse models for anticancer drug discovery and evaluation: a bridge to the clinic. Invest New Drugs. 1999; 17:343–359. [PubMed: 10759402]
10. Kim S, Park YW, Schiff BA, Doan DD, Yazici Y, Jasser SA, Younes M, Mandal M, Bekele BN, Myers JN. An orthotopic model of anaplastic thyroid carcinoma in athymic nude mice. Clin Cancer Res. 2005; 11:1713–1721. [PubMed: 15755992]
11. Bouvet M, Wang J, Nardin SR, Nassirpour R, Yang M, Baranov E, Jiang P, Moossa AR, Hoffman RM. Real-time optical imaging of primary tumor growth and multiple metastatic events in a pancreatic cancer orthotopic model. Cancer Res. 2002; 62:1534–1540. [PubMed: 11888932]
12. Hoffman RM. The multiple uses of fluorescent proteins to visualize cancer *in vivo*. Nat Rev Cancer. 2005; 5:796–806. [PubMed: 16195751]
13. Yang M, Baranov E, Jiang P, Sun FX, Li XM, Li L, Hasegawa S, Bouvet M, Al-Tuwaijri M, Chishima T, Shimada H, Moossa AR, Penman S, Hoffman RM. Whole-body optical imaging of green fluorescent protein-expressing tumors and metastases. Proc Natl Acad Sci USA. 2000; 97:1206–1211. [PubMed: 10655509]
14. Katz MH, Takimoto S, Spivack D, Moossa AR, Hoffman RM, Bouvet M. A novel red fluorescent protein orthotopic pancreatic cancer model for the preclinical evaluation of chemotherapeutics. J Surg Res. 2003; 113:151–160. [PubMed: 12943825]
15. Gomez-Rivera F, Santillan-Gomez AA, Younes MN, Kim S, Fooshee D, Zhao M, Jasser SA, Myers JN. The tyrosine kinase inhibitor, AZD2171, inhibits vascular endothelial growth factor receptor signaling and growth of anaplastic thyroid cancer in an orthotopic nude mouse model. Clin Cancer Res. 2007; 13:4519–4527. [PubMed: 17671138]
16. Kim S, Prichard CN, Younes MN, Yazici YD, Jasser SA, Bekele BN, Myers JN. Cetuximab and irinotecan interact synergistically to inhibit the growth of orthotopic anaplastic thyroid carcinoma xenografts in nude mice. Clin Cancer Res. 2006; 12:600–607. [PubMed: 16428506]
17. Kim S, Yazici YD, Barber SE, Jasser SA, Mandal M, Bekele BN, Myers JN. Growth inhibition of orthotopic anaplastic thyroid carcinoma xenografts in nude mice by PTK787/ZK222584 and CPT-11. Head Neck. 2006; 28:389–399. [PubMed: 16388530]
18. Kim S, Yazici YD, Calzada G, Wang ZY, Younes MN, Jasser SA, El-Naggar AK, Myers JN. Sorafenib inhibits the angiogenesis and growth of orthotopic anaplastic thyroid carcinoma xenografts in nude mice. Mol Cancer Ther. 2007; 6:1785–1792. [PubMed: 17575107]

19. Prichard CN, Kim S, Yazici YD, Doan DD, Jasser SA, Mandal M, Myers JN. Concurrent cetuximab and bevacizumab therapy in a murine orthotopic model of anaplastic thyroid carcinoma. Laryngoscope. 2007; 117:674–679. [PubMed: 17429874]
20. Wang Z, Chakravarty G, Kim S, Yazici YD, Younes MN, Jasser SA, Santillan AA, Bucana CD, El-Naggar AK, Myers JN. Growth-inhibitory effects of human anti-insulin-like growth factor-I receptor antibody (A12) in an orthotopic nude mouse model of anaplastic thyroid carcinoma. Clin Cancer Res. 2006; 12:4755–4765. [PubMed: 16899627]
21. Ahn SH, Henderson Y, Kang Y, Chattopadhyay C, Holton P, Wang M, Briggs K, Clayman GL. An orthotopic model of papillary thyroid carcinoma in athymic nude mice. Arch Otolaryngol Head Neck Surg. 2008; 134:190–197. [PubMed: 18283163]
22. Bouvet M, Spernyak J, Katz MH, Mazurchuk RV, Takimoto S, Bernacki R, Rustum YM, Moossa AR, Hoffman RM. High correlation of whole-body red fluorescent protein imaging and magnetic resonance imaging on an orthotopic model of pancreatic cancer. Cancer Res. 2005; 65:9829–9833. [PubMed: 16267005]
23. Snyder CS, Kaushal S, Kono Y, Tran Cao HS, Hoffman RM, Bouvet M. Complementarity of ultrasound and fluorescence imaging in an orthotopic mouse model of pancreatic cancer. BMC Cancer. 2009; 9:106. [PubMed: 19351417]
24. Hoffman RM, Yang M. Subcellular imaging in the live mouse. Nature Protocols. 2006; 1:775–782.
25. Nucera C, Nehs MA, Mekel M, Zhang X, Hodin R, Lawler J, Nose V, Parangi S. A novel orthotopic mouse model of human anaplastic thyroid carcinoma. Thyroid. 2009; 19:1077–1084. [PubMed: 19772429]
26. Schweppe RE, Klopper JP, Korch C, Pugazhenthi U, Benezra M, Knauf JA, Fagin JA, Marlow LA, Copland JA, Smallridge RC, Haugen BR. Deoxyribonucleic acid profiling analysis of 40 human thyroid cancer cell lines reveals cross-contamination resulting in cell line redundancy and misidentification. J Clin Endocrinol Metab. 2008; 93:4331–4341. [PubMed: 18713817]
27. Chambers AF. MDA-MB-435 and M14 cell lines: identical but not M14 melanoma? Cancer Res. 2009; 69:5292–5293. [PubMed: 19549886]
28. Zhang Q, Fan H, Shen J, Hoffman RM, Xing HR. Human breast cancer cell lines co-express neuronal, epithelial, and melanocytic differentiation markers *in vitro* and *in vivo*. PLoS One. 2010; 5:e9712. [PubMed: 20300523]
29. Weber CJ, Marvin M, Krekun S, Koschitzky T, Karp F, Benson M, Feind CR. Effects of tamoxifen and somatostatin analogue on growth of human medullary, follicular, and papillary thyroid carcinoma cell lines: tissue culture and nude mouse xenograft studies. Surgery. 1990; 108:1065–1071. [PubMed: 1978945]
30. Frasca F, Vigneri P, Vella V, Vigneri R, Wang JY. Tyrosine kinase inhibitor STI571 enhances thyroid cancer cell motile response to Hepatocyte Growth Factor. Oncogene. 2001; 20:3845–3856. [PubMed: 11439348]
31. Vella V, Zhu J, Frasca F, Li CY, Vigneri P, Vigneri R, Wang JY. Exclusion of c-Abl from the nucleus restrains the p73 tumor suppression function. J Biol Chem. 2003; 278:25151–25157. [PubMed: 12716888]
32. Ma H, Li X, Yang Z, Okuno S, Kawaguchi T, Yagi S, Bouvet M, Hoffman RM. High antimetastatic efficacy of MEN4901/T-0128, a novel camptothecin carboxymethyldextran conjugate. J Surg Res. Jun 25.2010 Epub ahead of print.
33. Li X, Wang J, An Z, Yang M, Baranov E, Jiang P, Sun F, Moossa AR, Hoffman RM. Optically imageable metastatic model of human breast cancer. Clin Exp Metastasis. 2002; 19:347–350. [PubMed: 12090475]
34. Yang M, Li L, Jiang P, Moossa AR, Penman S, Hoffman RM. Dual-color fluorescence imaging distinguishes tumor cells from induced host angiogenic vessels and stromal cells. Proc Natl Acad Sci USA. 2003; 100:14259–14262. [PubMed: 14614130]
35. Togo S, Shimada H, Kubota T, Moossa AR, Hoffman RM. Host organ specifically determines cancer progression. Cancer Res. 1995; 55:681–684. [PubMed: 7834640]

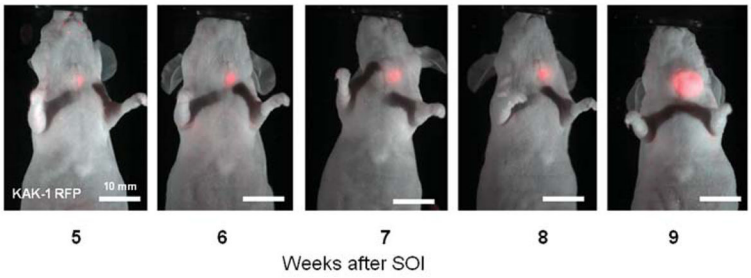

Figure 1.

Real-time imaging of tumor growth in a mouse bearing a KAK-1-RFP tumor over time. Brightfield images and fluorescence images obtained by the monochrome camera were superimposed. In this particular animal, the tumor first became visible on week 5 post-implantation but was not palpable until week 7 after surgical implantation. Weekly imaging allowed monitoring and documentation of tumor growth until the animals were sacrificed. The median time to non-invasive tumor detection via fluorescence for KAK-1-RFP tumors was postoperative week 5, that for NPA-1-RFP was postoperative week 9.

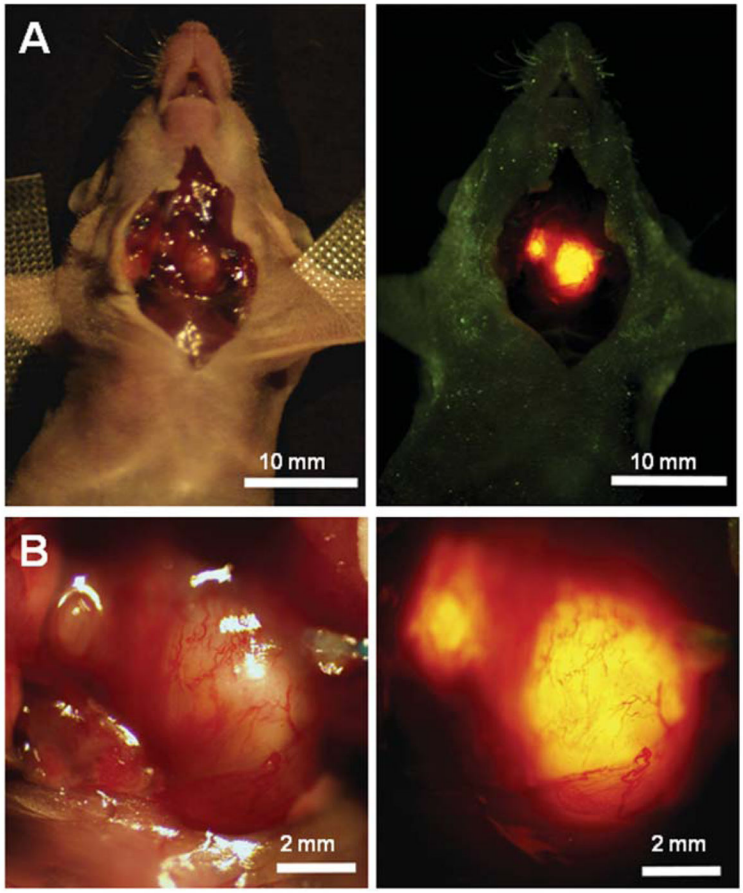

Figure 2.

RFP-expressing orthotopic tumors emit a brightly fluorescent signal with proper excitation. Imaging of the exposed neck of the mouse permitted rapid identification of separate tumors in the two thyroid lobes. The signal was intense and facilitated tumor detection. This mouse demonstrates bilateral tumor foci that developed following orthotopic implantation of RFP-expressing NPA thyroid cancer cells. Left panels are brightfield images and right panels are fluorescense images.

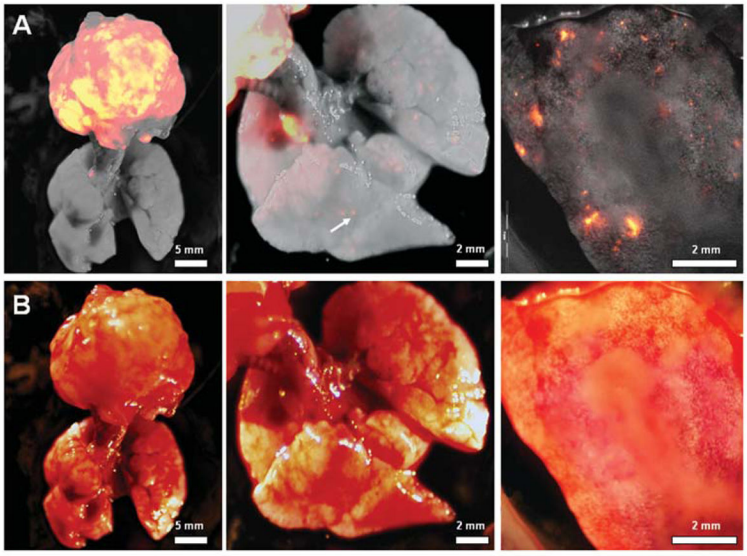

Figure 3.

Fluorescence imaging of metastases. For both KAK-1 and NPA tumors, metastases developed after extended tumor growth. A: Fluorescence imaging of a thyroid/tumor/lung organ block which demonstrated paratracheal lymph node metastases (middle panel) and disseminated pulmonary micrometastases (right panel). B: Imaging of the same specimen under bright light failed to reveal the presence of metastatic disease, especially in the lung parenchyma.

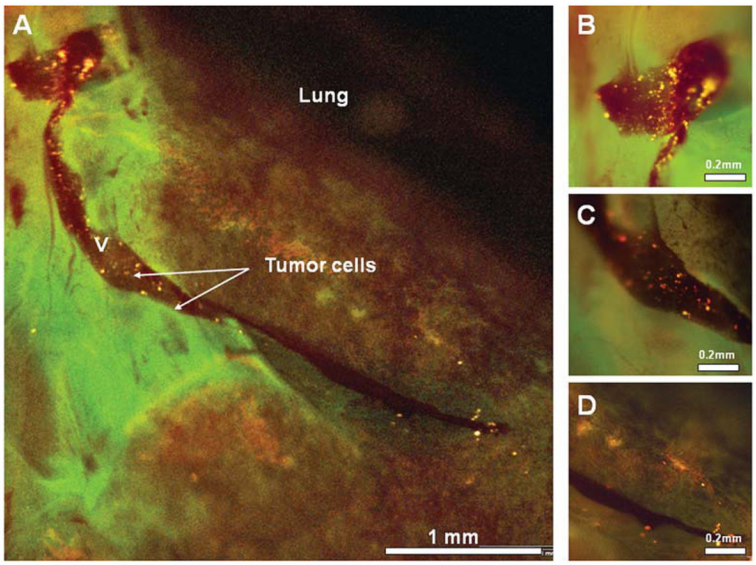

Figure 4.

High magnification fluorescence images of the lung (panel A). KAK-1-RFP cells were identified via fluorescence imaging within a superficial vascular channel (magnified views, panels B–D) traversing the pleural surface of the lung parenchyma.

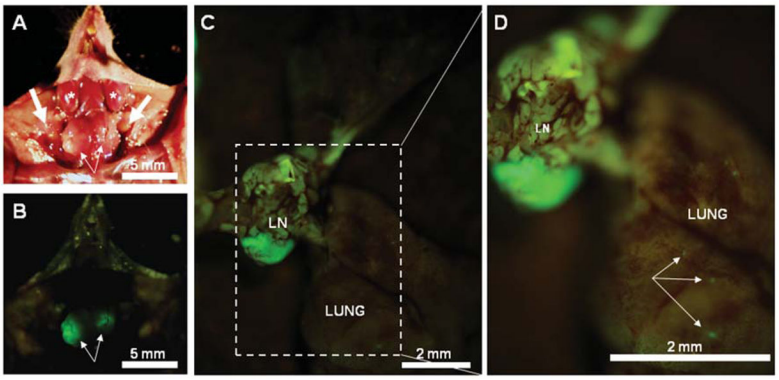

Figure 5.

Intravital fluorescence imaging of GFP-expressing KAK-1 tumors. In this orthotopic KAK-1-GFP-bearing animal. Imaging under fluorescence light clearly identified the tumor (thin arrows) (B), differentiating it from other structures within the neck of the mouse, including the cheek muscles (*) and salivary glands (thick arrows) (A). Once the thyroid/tumor/lung organ block was resected, a metastatic lesion was seen in the paratracheal lymph node (LN), right above the lungs, at moderate magnification (C). At higher magnification of the outlined area in panel C, additional small metastatic deposits became visible within the lungs (arrows) due to their fluorescent signal (D).

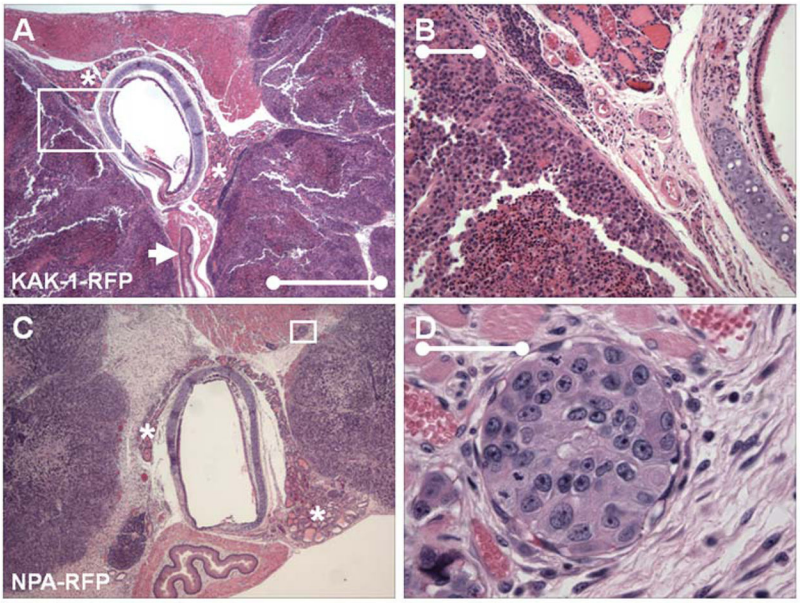

Figure 6.

Histological appearance of KAK-1-RFP and NPA-RFP primary thyroid tumors. Transverse sections of KAK-1-RFP (A and B) and NPA-RFP (C and D) primary thyroid tumors show the relationships of bilateral tumor masses with residual normal thyroid (*) and adjacent tissues. KAK-1-RFP thyroid cancer cells formed large, centrally necrotic masses that distorted and compressed adjacent structures such as the esophagus (arrow in A, 2×, scale bar=1 mm). Higher magnification (B, ×10, scale bar=100 microns) of the area indicated in (A) gives a closer view of the tumor (left), the trachea (right), and normal residual thyroid tissue (upper middle). As compared to KAK-1-RFP, NPA-RFP thyroid cancer cells formed smaller tumor masses (C) and demonstrated more evidence of differentiation and a propensity for involvement of small vascular structures (inset area in C; higher magnification in D, ×40, scale bar=50 micron).